THEORETICA CHIMICA ACTA
Theoret. Chim. Acta (Berl.) 59, 555–568 (1981)

Original Investigations

The Band Structures and Magnetic Properties of Some Transition-metal Monophosphides I. Scandium Phosphide

Peter G. Perkins, Ashok K. Marwaha, and James J. P. Stewart

Department of Pure and Applied Chemistry, University of Strathclyde, Glasgow G1 1XL, Scotland

An improved method is described for the calculation of the band structures and density of states for three-dimensional solids. It is based on an LCAO-TB method. The method is applied to the scandium phosphide crystal. This material is calculated to be a semiconductor with a small band gap.

Key words: Band Structure – Binary phosphides – Electronic properties.

1. Introduction

This is the first of two papers dealing with the electronic band structures of some transition-metal phosphides. In the present paper we develop an improved LCAO tight-binding method and apply it to the case of scandium phosphide and in the second paper we will examine other transition-metal monophosphides.

Previous work [1, 2, 3] has shown that a simple LCAO approach to electronic band-structure calculation can yield satisfyingly consistent results for the electronic structures of metal borides. The approach is here extended to a consideration of some bindary phosphides.

The phosphides of transition-metal elements exhibit considerable variation in crystal structure and stoichiometry. They also show interesting electrical and magnetic properties. Although certain qualitative explanations [4, 5] have been given for their properties, before we started the present work no band-structure calculations of these compounds had been carried out. However, during the course of the work a report on a calculation of the band structure of scandium phosphide became available [6]. In the present work we have studied certain of

0040-5744/81/0059/0555/$02.80

the monophosphides of the 3*d* transition elements, the choice being based on the simplicity of their crystal structures and on the availability of data appertaining to their properties. Thus, of the 3*d* monophosphides, ScP is reported to be a semiconductor with a band gap of 1.1 eV [7] whilst the others in the series are metal-like, with electrical conductivities comparable with those of some metals [8]. Of these materials only MnP has been shown to be magnetic below 292 K, while all other members of the series are non-magnetic and only possess weak Pauli paramagnetism [5]. An attempt is made here and in the second paper to rationalise these observations.

2. Calculational Method

2.1. Band Structure and Density of States

The method used for band-structure calculations was based on an Extended-Hückel formulation previously described [1]. Considerable progress in the implementation of this method has, however, been made and some description is therefore given here. Input atomic data (orbital exponents and valence-state ionization potentials for the basis functions) are given in Table 1 for scandium and phosphorus. The data for the latter element have been employed in many previous molecular calculations [9, 10].

For ScP there is one molecule per unit cell, whilst in VP there are two and in MnP and CrP there are four. In the latter cases, the number of valence orbitals amounts to 72 if the empty phosphorus 3*d* orbitals are included. This size of basis set is unmanageable and, hence, we were constrained to omit the phosphorus 3*d* orbitals in all cases. This will be commented on in a later context. In all cases the Mulliken–Wolfsberg–Helmholtz scaling factor for the off-diagonal matrix elements between atomic orbitals was set at 2.0.

When such large basis sets are used in a calculation, there ensues the problem of correctly connecting up the points in ***k***-space given by the calculation and correctly identifying crossing points. This is an impossible task by hand, particularly in the region of the Fermi level where the states are closely aggregated. Hence, the plotting of bands along the symmetry directions was carried out by an automatic procedure. The background to this procedure is as follows.

Table 1. Input data for the atoms

	Exponents				VSIP			
	4*s*		4*p*	3*d*	4*s*		4*p*	3*d*
Sc[b]		0.975	0.65	2.067		5.70	3.22	4.71
P[a]	(3*s*)	1.75	(3*p*) 1.30	0.667	(3*s*)	19.37	(3*p*) 10.84	1.45

[a] Ref. [20].
[b] Calculated from atomic spectra in the usual way [20].

The orbitals of a crystal form an orthonormal set as,

$$\langle \psi_i(\boldsymbol{k}) | \psi_j(\boldsymbol{k}') \rangle = \delta_{ij}\delta_{\boldsymbol{k}\boldsymbol{k}'}. \tag{1}$$

However, if the wave vectors $\boldsymbol{k}$ and $\boldsymbol{k}'$ are separated by a small distance $\delta\boldsymbol{k}$ in the reciprocal space, one can use perturbation theory to calculate the integral S'_{ij} as:

$$\begin{aligned} S'_{ij} &= \langle \psi_i(\boldsymbol{k}) | \delta_{\boldsymbol{k}} | \psi_j(\boldsymbol{k}') \rangle \\ &= \langle \psi_i(\boldsymbol{k}) | \psi_j(\boldsymbol{k}) \rangle. \end{aligned} \tag{2}$$

The value of S'_{ij}will be largest for the wavefunctions $\psi_i(\boldsymbol{k})$ and $\psi_j(\boldsymbol{k}')$, if they both correspond to eigenvalues originating in the same band.

We have,

$$\psi_i(\boldsymbol{k}) = \sum_{\lambda} C_{\lambda i}(\boldsymbol{k}) \phi_{\lambda}^{\boldsymbol{k}} \tag{3}$$

$$\psi_j(\boldsymbol{k}) = \sum_{\lambda} C_{\lambda j}(\boldsymbol{k}') \phi_{\lambda}^{\boldsymbol{k}'}. \tag{4}$$

If $\boldsymbol{k}$ and $\boldsymbol{k}'$ are very close to each other in the Brillouin Zone, then,

$$\begin{aligned} S'_{ij} &= \sum c^*_{\lambda i}(\boldsymbol{k}) c_{\lambda j}(\boldsymbol{k}') \\ &= \sum_{\lambda} (R_{c_{\lambda i}(\boldsymbol{k})} - iI_{C_{\lambda i}(\boldsymbol{k})})(R_{c_{\lambda j}(\boldsymbol{k}')} + iI_{c_{\lambda j}(\boldsymbol{k}')}) \end{aligned} \tag{5}$$

where $R_{c_{\lambda i}}$ and $I_{c_{\lambda i}}$ are the real and imaginary parts of the coefficients $c_{\lambda i}(\boldsymbol{k})$,

$$S'_{ij} = R_c + iI_c. \tag{6}$$

One can calculate the modulus of this complex number as,

$$|S'_{ij}| = \sqrt{R_c^2 + I_c^2}. \tag{7}$$

$|S'_{ij}|$ can be related to the overlap between the two state functions $\psi_i(\boldsymbol{k})$ and $\psi_j(\boldsymbol{k}')$ of a crystal. Hence, one can connect the pairs of eigenvalues to form a band for two near neigbouring $\boldsymbol{k}$-points if S'_{ij} between the corresponding crystal orbitals is a maximum. This criterion establishes the correct compatibility relation between the eigenvalues of the crystal.

A complete description of the band structure requires the knowledge of the symmetry properties of the bands at special points and along the lines of symmetry in the Brillouin zone. Therefore, it is necessary to calculate the expectation values of the compound symmetry operators $\{\hat{R}_\alpha | \hat{\omega}_\alpha + \hat{R}_n\}$ (i.e. $\langle \psi_i(\boldsymbol{k})^* | \{\hat{R}_\alpha | \hat{\omega}_\alpha + \hat{R}_n\} | \psi_i(\boldsymbol{k}) \rangle$) belonging to G^k, the little group of the wave vector at these symmetry points and along the lines of symmetry in the Brillouin zone.

This procedure is followed through automatically in the program and, hence, a complete definition of the symmetry of the bands is afforded.

2.2. *The Density-of-States Function*

The density-of-states and related functions were obtained using linear interpolation techniques. Our method is somewhat different from those previously used and hence a description is given here.

The density-of-states function $g_j(E)$, defined as the number of available states per unit volume per unit energy interval for band j, is given by,

$$g_j(E) = \frac{2}{8\pi^3} \int \delta\{\varepsilon_j(\boldsymbol{k}) - E\}\, d\boldsymbol{k} \tag{8}$$

in the form,

$$\bar{g}_j = \frac{2}{N_p} \frac{1}{\Delta E} \sum_{i=1}^{N_p} \Delta_j(\boldsymbol{k}_i) \tag{9}$$

where $\Delta_j(\boldsymbol{k}_i)$ is unity if $\varepsilon_j(\boldsymbol{k}_i)$ is within an interval ΔE about E, zero otherwise, and $\boldsymbol{k}_i$ are the sampling points in the first Brillouin Zone of the system. The total density of states arising from all the bands of the system is then,

$$G(E) = \sum_{\text{all bands}} \bar{g}_j(E). \tag{10}$$

The standard numerical technique for the evaluation of Eq. (9) is to obtain the eigenvalues associated with a commensurate mesh of $\boldsymbol{k}$-points lying in the representation domain Φ of the Brillouin Zone and then to generate a fine mesh of k-points and the associated eigenvalues using linear interpolation techniques. Finally, the density-of-states function for the jth band is calculated as:

$$\bar{g}_j(E) = \frac{2}{N_p} \frac{1}{\Delta E} \sum_{i=1}^{N_A} \omega_i \Delta_j(\boldsymbol{k}_i) \tag{11}$$

where ω_i is the star of the wave vector $\boldsymbol{k}_i$ and N_p is the normalising constant given by:

$$N_p = \sum_{i=1}^{N_A} \omega_i. \tag{12}$$

In our method, in place of the representation domain Φ of the Brillouin Zone, a cubic fraction of the zone volume is employed such that the resulting $\boldsymbol{k}$-points have the star of unity, thereby improving the sampling quality of the interpolated $\boldsymbol{k}$-points and the associated eigenvalues. Therefore, as the first step towards calculating $G(E)$, we define the representative domain Φ_R as the volume in reciprocal space such that $\sum_{\hat{R}_\beta} \hat{R}_\beta \Phi_R$ is equal to an integral multiple of the first Brillouin Zone volume and, furthermore, the volume produced above can be divided into an integral number of cubes. The sum over $\hat{R}_\beta$ extends over the elements of the holosymmetric point group P of the lattice. We shall refer to this reciprocal space volume hereafter as the NBZ volume. Fig. 1 shows the

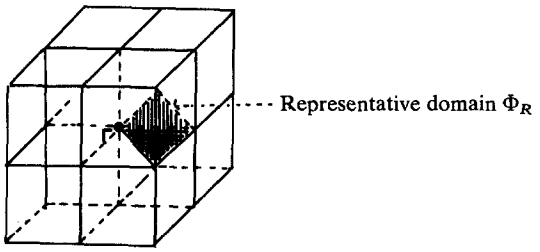

Fig. 1. Representative domain Φ_R for cubic lattices

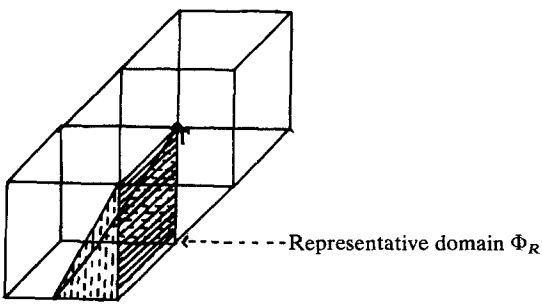

Fig. 2. Representative domain Φ_R for the hexagonal lattice

representative domain Φ_R for cubic lattices and the final NBZ volume divided into eight equivalent cubes, while Fig. 2 gives the representative domain Φ_R for hexagonal into three equivalent cubes.

We calculate an approximate $G(E)$ in crystals by obtaining the eigenvalues associated with a commensurate mesh of $\boldsymbol{k}$-points in the representative domain Φ_R of the system. The symmetry operations of the point group P of the lattice are then used to produce the equivalent wave vectors and the associated eigenvalues in the NBZ volume. From this NBZ volume, we select one of the integral cubic fractions. This cube is like a finite simple cubic lattice, where each k-point is a unit cell of this finite lattice. We use three unit cells to generate new wave vectors and associated eigenvalues required for calculation of $G(E)$. Thus, let $E_j(0, 0, 0)$, $E_j(0, 0, 1), \ldots, E_j(1, 1, 1)$ be the supplied energy of the jth band at positions $(0, 0, 0), (0, 0, 1), \ldots, (1, 1, 1)$ of one of new cubes described above. Then the energy $E_j(k_{x_A} k_{y_A} k_{z_A})$ at the generated $\boldsymbol{k}$-point $k_{x_A} k_{y_A} k_{z_a}$ is given by

$$E_j(k_{x_A}, k_{y_A}, k_{z_A}) = E(XX') + ns[E(YX') - E(XX')]S \tag{13}$$

where ns varies from 1 to NS, NS being the number of steps used for interpolation in each direction of the cube and S is the step size.

The energies $E_j(XX)$ and $E_j(YX)$ are generated in terms of $E_j(0, 0, 0)$, $E_j(0, 0, 1), \ldots E_j(1, 1, 1)$ as:

$$E_j(XX') = E_j(XX) - \tfrac{1}{3}[E_j(XY) - E_j(XX)]S + ns[E_j(XY) - E_j(XX)]S$$

$$E_j(YX') = E_j(YX) - \tfrac{1}{3}[E_j(YY) - E_j(YX)]S + ns(E_j(YY) - E_jYX)]S$$

where $E_j(XX)$, $E(YX)$, and $E_j(YY)$ are given by,

$$E_j(XX) = E_j(000) - \tfrac{2}{3}[E_j(001) - E_j(000)]S + ns[E_j(001) - E_j(000)]S$$

$$E_j(XY) = E_j(010) - \tfrac{2}{3}[E_j(011) - E_j(010)]S + ns[E_j(011) - E_j(010)]S$$

$$E_j(YX) = E_j(100) - \tfrac{2}{3}[E_j(101) - E_j(100)]S + ns[E_j(101) - E_j(100)]S$$

$$E_j(YY) = E_j(110) - \tfrac{2}{3}[E_j(111) - E_j(110)]S + ns[E_j(111) - E_j(110)]S.$$

Fig. 3 shows such an interpolation scheme carried out for generating three points in each direction of the cube. The generated points are marked X. As shown in Fig. 3, all generated points avoid any special symmetry positions, thus improving the sampling quality. This is done for all the unit cells of the cube obtained from the NBZ volume. Thus, an approximate form of $\bar{g}_j(E)$ can be obtained from Eq. (14) and is written as,

$$\bar{g}_j(E) = \frac{1}{N_p} \frac{1}{\Delta E} \sum_{i=1}^{N_p} \Delta_j(\boldsymbol{k}_i) \tag{14}$$

where summation of i runs over the points generated in the cubic fraction of NBZ volume. The periodic properties of the reciprocal space ensure the correct behaviour of $\bar{g}_j(E)$ after normalisation.

Finally, the total density of states is calculated using Eq. (11).

2.3. The Joint-Density-of-States Function

The density-of-states function $G(E)$ furnishes information on the location of electronic states in crystals. It can further be used to obtain a qualitative picture of electronic transitions in crystals.

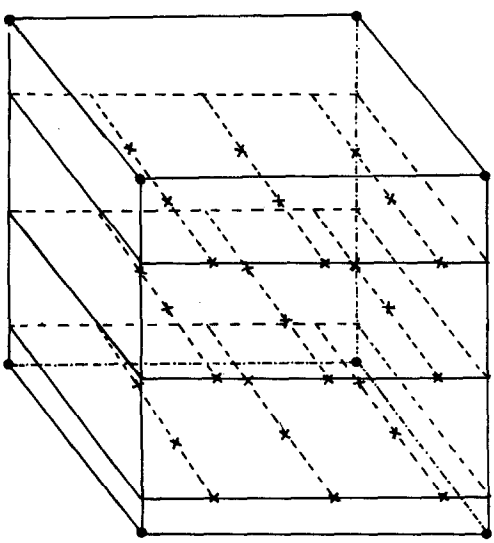

Fig. 3. Supplied (·) and generated (×) $\boldsymbol{k}$-points from the interpolation scheme

The imaginary part of the complex dielectric function $\varepsilon_2(\omega)$, related to the electronic transitions in crystals, is given by Eq. (15),

$$\varepsilon_2(\omega) = 2\frac{e^2h^2}{m}\sum_{c,v}\frac{1}{8\pi^3}\int f_{cv}(\boldsymbol{k})^{\delta}\frac{(E_c - E_v - h\omega)}{E_{cv}(\boldsymbol{k})} \tag{15}$$

where c and v are labels for conduction and valence bands, respectively, $E_{cv} = E_c(\boldsymbol{k}) - E_v(\boldsymbol{k})$ and $f_{cv}(\boldsymbol{k})$ is the interband oscillator strength which characterises the transition probability between $\psi_c(\boldsymbol{k})$ and $\psi_v(\boldsymbol{k})$. The complete evaluation of $\varepsilon_2(\omega)$ is complicated by the presence of $f_{cv}(\boldsymbol{k})$, the oscillator strength, in the equation. However, we can approximate the joint-density-of-states function, JDOS(E), representing the available interband transitions, in exactly the same way as the density of states $G(E)$, thus,

$$\text{JDOS}(E) = \frac{1}{\Delta E}\frac{1}{N_p}\sum_{i=1}^{N_p}\Delta[\{E_c(\boldsymbol{k}_i) - E_v(\boldsymbol{k}_i)\} - E]. \tag{16}$$

Furthermore, as required, we can remove the restriction of $\boldsymbol{k}$-conservation and can calculate a joint-density-of-states function (J'DOS(E)) using the density-of-states function $G(E)$ thus,

$$\text{J'DOS}(E) = \sum_{c,v} G(E_c) \times G(E_v) \cdot \Delta((E_c - E_v) - E) \tag{17}$$

where $G(E_c)$, $G(E_v)$ are the total density of states at energy E_c and E_v, respectively, in the conduction and the valence bands lying either side of the Fermi level.

The functions JDOS(E) and J'DOS(E) can deviate somewhat from $\varepsilon_2(\omega)$; nevertheless, from them one can obtain a semi-quantitative picture of the possible electronic transitions in the solid.

3. Results and Discussion

As aforestated in this paper, we consider here only the case of ScP, the only reported semi-conductor in the series.

3.1. Band Structure for ScP

The primitive unit cell of ScP consists of an Sc atom at (0, 0, 0) and a P atom at (0, 0, $a/2$), and interactions between 135 unit cells of the lattice (second nearest neighbours) were taken into account in the calculations. The lattice constant is 0.5312 nm [11] and the space group O_h^5. The first Brillouin Zone for the face-centred cubic lattice is shown in Fig. 4, with standard notation for the high-symmetry points.

Fig. 5 shows the band structure around the Fermi level along the lines $\Gamma - X - W - L - \Gamma - K - X$. We note that there is a similarity between the band structure of ScP and those ScC and ScN [12] and TiO, TiN [13]. Near Γ, the valence-band states arise principally from the 3s and 3p orbitals of phosphorus, but, as the wave vector $\boldsymbol{k}$ increases from Γ, the metal orbitals also contribute

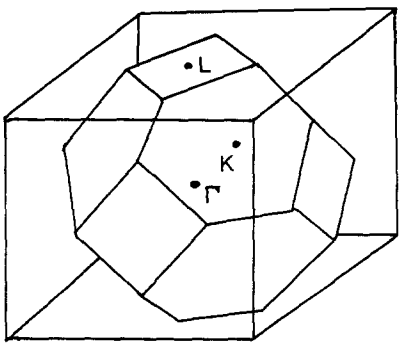

Fig. 4. Brillouin zone for face-centred-cubic lattice

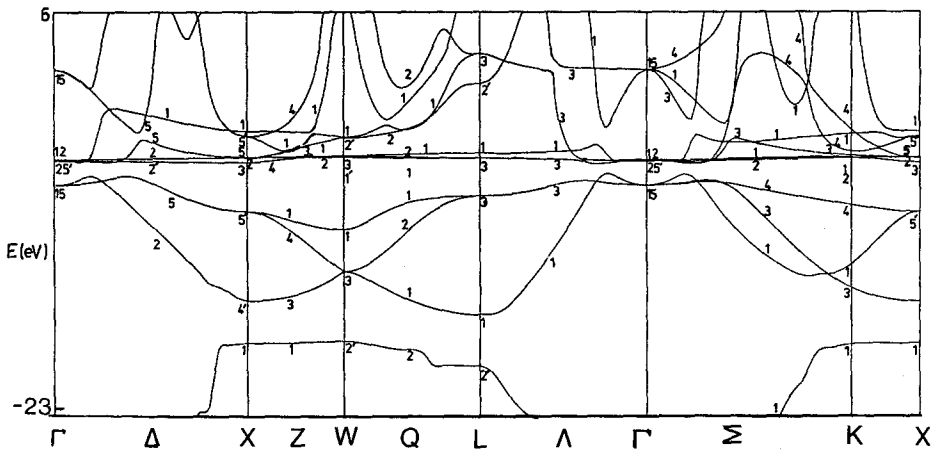

Fig. 5. Band structure for ScP

significantly to these valence bands. Table 2 shows the composition of the valence bands at the special symmetry points in the Brillouin Zone. In our calculation the eight valence electrons per unit cell completely fill the valence band, after which there is a band gap of 0.80 eV between the highest filled valence band and the lowest-lying conduction band. The latter occurs along the symmetry line $\Gamma - K$ in the Brillouin Zone. The conduction band consists mainly of states arising from the metal 4*s*, 4*p*, and 3*d* orbitals. Actually, the bands which stem from the metal 4*s* and 4*p* orbitals lie higher in energy whilst, at the bottom of the conduction band, the bands arising from the metal 3*d* orbitals spread over an energy range of about 4.0 eV. The narrowness of the individual metal 3*d* bands in the lower conduction region implies large effective electron masses.

Our calculation does not include the 3*d* orbitals of phosphorus. We did, however, investigate their influence by means of a periodic cluster approach [14, 15]. This yielded the eigenvalues corresponding to the band structure at Γ and *X*. The input data representing the phosphorus 3*d* orbitals are given in Table 1. Briefly,

Table 2. Composition of the valence band in ScP at special symmetry points

Energy (eV)	Symmetry	Composition
−23.35	Γ_1	100% 3*s* (P)
−6.55	Γ_{15}	100% 3*p* (P)
−17.98	X_1	95% 3*s* (P), 5% 3*d* (Sc)
−14.92	X'_4	96% 3*p* (P), 4% 4*p* (Sc)
−8.46	X'_5	100% 3*p* (P)
−19.65	L'_2	94% 3*s* (P), 6% 4*p* (Sc)
−15.91	L_1	93% 3*p* (P), 6% 4*s* (Sc)
−7.31	L_3	42.5% 3*p* (P), 57.4% 3*d* (Sc)
−17.85	W'_2	96% 3*s* (P), 4% 3*d* (Sc)
−12.78	W_3	98% 3*p* (P), 2% 3*d* (Sc)
−9.75	W_1	86% 3*p* (P), 12% 3*d* (Sc)

the results of this treatment are: the phosphorus 3*d* orbitals enter the band scheme in the low conduction band area and decrease the band-gap at Γ by ~0.1 eV. (We cannot judge its effect between Γ and K from a "small cluster" calculation [14].) Hence, the *d* orbitals of phosphorus do not remove the band gap for ScP.

Recent calculations of the band structure of ScP by the APW method with exchange-correlation predict the material to be a metallic conductor [6]. The occurrence of an optical band gap [7] is put down by these authors as stemming from transitions from P(3*p*) to Sc(3*d*) orbitals. The true nature of this material, therefore, is somewhat puzzling since, on the one hand, the above APW method has previouly afforded accurate, physically sensible, and consistent results on a variety of similar binary materials [12, 13, 16] and, moreover, the experimental observation on ScP was an optical rather than a thermal band-gap determined by conductivity changes. (Actually, a thermal band-gap could not be measured for the prepared materials because of donor impurities, *vide infra.*)

On the other hand, the work in Ref. [7] reports not only the band gap for ScP but also a sharp optical band gap for the closely related compound ScAs. Moreover, independently, Sclar [17] also suggested a value of 1.45 eV for ScP. Optical band-gap measurement is a well-established technique and may be in some ways more reliable than conductivity studies. Furthermore, the band-gap evidence does not stand by itself; measurements of the Hall effect lead to values of the Hall mobility of 10–30 $cm^2\ V^{-1}\ sec^{-1}$ [7] with a carrier concentration of $2\times10^{21}\ cm^{-3}$.

The samples of ScP and ScAs prepared and examined by Yim et al. were highly *n*-type, with a carrier concentration in the region of $10^{21}\ cm^{-3}$. Moreover, they detected no metal impurities or phosphorus but rather large concentrations of chlorine (10^2–10^4 at p.p.m.) It seems very likely that the *n* character of the materials stem from these chlorine impurities having donor levels lying just below the conduction band edge.

The sign and magnitude of the Hall constants, the magnitude of the hall mobility for the carriers, and the measured electrical conductivity for ScAs [7] are all completely consistent with the above interpretation. The Seebeck coefficient is also large and negative [7] and indicates the carriers to be electrons as in a low-band-gap semiconductor.

The electrical conductivity of ScAs is of the same order as that of graphite [18] which, in the region of the Fermi level, also has a small gap. The conductivity of ScAs is about three orders of magnitude too low for a metallic conductor. Hence, the only possibility to explain metallic behaviour is that the material is further impure in some undetected way. Since impurities in materials generally induce *higher* conductance than the pure material because of n and p impurity levels, then it is difficult to see how a material which is really a metallic conductor can be turned into a semiconductor through impurities.

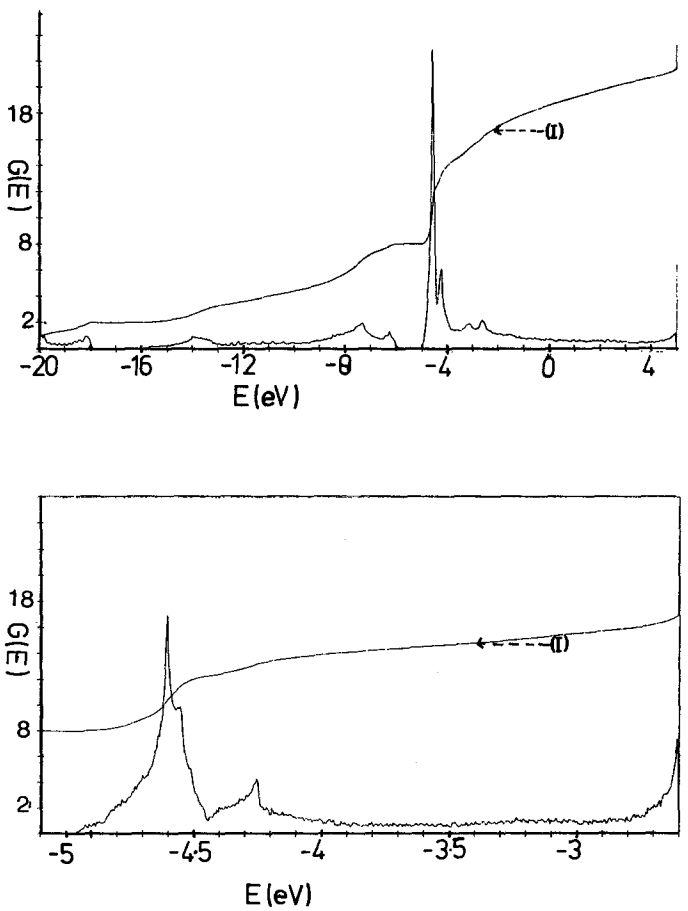

Fig. 6. Total density of states for ScP. The lower figure extends the scale in the band-gap region (I) is the integral of the density of states. The abscissa gives the number of electrons

3.2. *The Density-of-States and Related Functions in* ScP

The electronic density-of-states function obtained by linear interpolation of 230 $\boldsymbol{k}$-points in the representative domain Φ_R is shown in Fig. 6. The valence band has a gap of about 2 eV separating the states arising from $3s$ and $3p$ orbitals of phosphorus. Above the band gap, the bands arising from the $3d$ orbitals of scandium are seen. The effect of the crystal potential, essentially octahedral, on these $3d$ orbitals is well demonstrated in the band structure and the mixing and spreading of the atomic states arising from the orbitals of t_{2g} and e_g types give rise to peaks in the density of states having area ratio 3:2. These figures show that the absorption spectrum should show little change on disordering of the lattice in any way. The "t_{2g} band" peaks near −4.6 eV and the "e_g band" near −4.25 eV.

Finally, Figs. 7 and 8 show the joint-density-of-states functions J'DOS(E) and JDOS(E) calculated as previously described. Both of these show the fundamental absorption edge at about 0.80 eV and the other possible transitions in ScP.

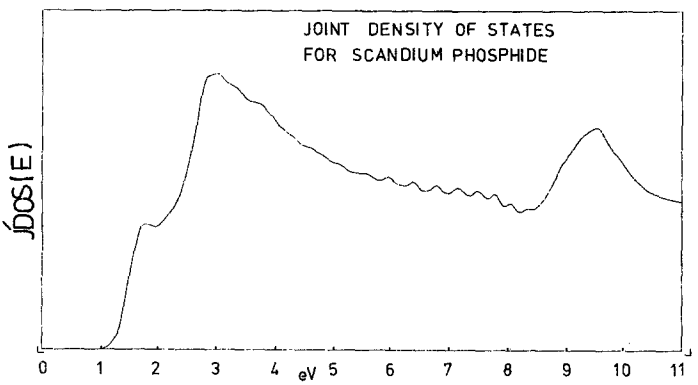

Fig. 7. Modified joint density of states function (J'DOS)

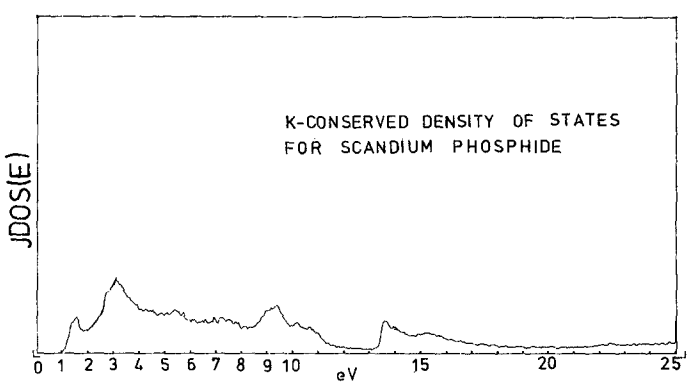

Fig. 8. Joint density of states function (JDOS)

3.3. Bonding and Charge Distribution in ScP

The computed partial densities of states for the basis orbitals of the unit cell are shown in Figs. 9 and 10. They afford a qualitative description of the bonding in crystalline ScP. The 4*s* orbitals on Sc, which are filled in the free atom, lie mainly in the conduction band and this results in the loss of 1.86 electrons from the metal. However, the 4*p* orbitals, which are formally empty, take part in the crystal bonding and gain ~0.37 electrons. The metal 3*d* orbitals (with one electron in the free atom) also increase their share of available electrons in the crystal by lowering their energy and gain ~0.44 electrons. The orbitals of phosphorus, though mainly of bonding type, also have some antibonding character and partially lie in the conduction band. Overall, the metal-ligand bonding in the crystal results in a charge separation of $Sc^{+1.14}\,P^{-1.14}$; this is to be compared

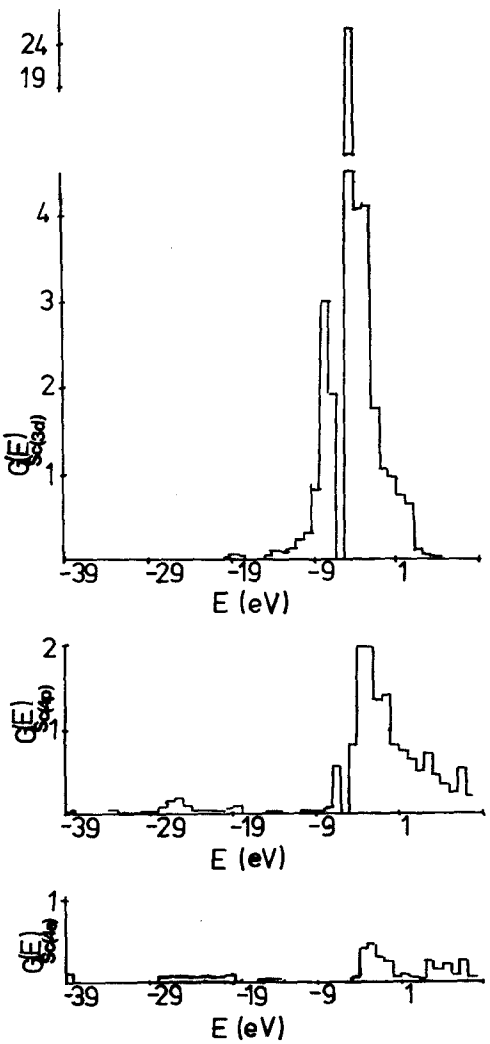

Fig. 9. Partial densities of states for Sc orbitals in ScP

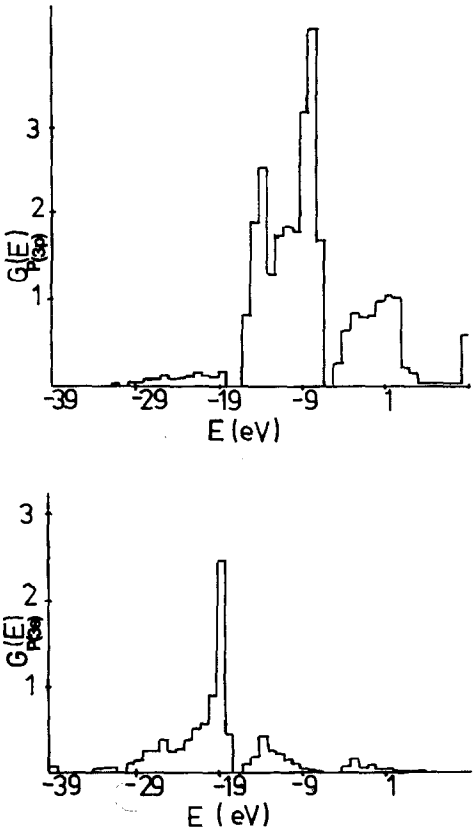

Fig. 10. Partial densities of states for P orbitals in ScP

with the formal oxidation states leading to $Sc^{3+}P^{3-}$ and so considerable covalent character is found. The bond index [19] for the ScP bond is 0.29 and for the nearest Sc–Sc it is 0.02. Since for a purely ionic bond the bond index must be zero [19], then a considerable degree of covalency is evident in the ScP bond. This covalency is partially responsible for the semi-conducting nature of the crystal; a "purely ionic" crystal would inevitably possess a far higher band gap but covalent mixing of the metal-ligand orbitals in the crystal reduces the band gap.

Acknowledgement. One of us (A.K.M.) thanks the University of Strathclyde for a Bursary.

References

1. Armstrong, D. R., Breeze, A., Perkins, P. G.: J. Physics (C), Solid State Physics **8**, 3558 (1975)
2. Armstrong, D. R., Breeze, A., Perkins, P. G.: J. Chem. Soc. (Lond.) Faraday Trans. II **73**, 952 (1977)
3. Armstrong, D. R., Perkins, P. G.: J. Chem. Soc. (Lond.) Faraday Trans. II **75**, 12 (1979)
4. Goodenough, J. B.: Phys. Rev. **117**, 1442 (1960) (and other unpublished work quoted in Ref. [5])

5. Stern, B. F., Walmsley, R. H.: Phys. Rev. **148**, 933 (1966)
6. Wimmer, E., Neckel, A., Schwarz, K.: 6th International Conference on Solid Compounds of Transition Elements, p. 44. Stuttgart, FRG: 1979
7. Yim, W. B., Stafko, E. J., Smith, R. J.: J. Applied Physics **43**, 254 (1972)
8. Ripley, R. L.: J. Less Common Metals **4**, 496 (1962)
9. See, for example, Armstrong, D. R., Easdale, M. C., Perkins, P. G.: Phosphorus **3**, 251 (1974)
10. McAloon, B. J., Perkins, P. G.: Theoret. Chim. Acta (Berl.) **22**, 304 (1971)
11. Parthe, E., Parthe, E.: Acta Cryst. **16**, 71 (1963)
12. Schwarz, K., Neckel, A., Weinberger, P.: Theoret. chim. Acta (Berl.) **15**, 149 (1969)
13. Neckel, A., Schwarz, K., Eibler, R., Weinberger, P., Rastl, P.: Berichte der Bunsen-Gesellschaft für physikalische Chemie 1053 (1975)
14. Perkins, P. G., Stewart, J. J. P.: J. Chem. Soc. (Lond.) Faraday Trans. II (in press)
15. Perkins, P. G., Stewart, J. J. P.: J. Chem. Soc. Faraday Trans. II (in press)
16. Schwarz, K.: J. Phys. (C) Solid State Physics **10**, 195 (1977): Neckel, A., Schwarz, K., Eibler, R., Rastl, P., Weinberger, P.: Mikrochim. Acta (Wien), Suppl. **6**, 257 (1975)
17. Sclar, N.: J. Applied Physics **33**, 2999 (1962)
18. Handbook of Physics and Chemistry, Chemical Rubber Publishing Company, ed. R. C. Weast (1977)
19. Armstrong, D. R., Perkins, P. G., Stewart, J. J. P.: J. Chem. Soc. Dalton Trans. 838 (1973)
20. Levison, K. A., Perkins, P. G.: Theoret. Chim. Acta (Berl.) **14**, 206 (1969)

Received September 25, 1980/March 6, 1981